Journal of Marine Research, 52, 773–796, 1994

Journal of
MARINE RESEARCH

Volume 52, Number 5

Parameter space exploration of an ocean general circulation model using an isopycnal mixing parameterization

by William A. Gough[1] and William J. Welch[2]

ABSTRACT

In this study we have employed statistical methods to efficiently design experiments and analyze output of an ocean general circulation model that uses an isopycnal mixing parameterization. Full ranges of seven inputs are explored using 51 numerical experiments. Fifteen of the cases fail to reach satisfactory equilibria. These are attributable to numerical limitations specific to the isopycnal model. Statistical approximating functions are evaluated using the remaining cases to determine the dependency of each of the six scalar outputs on the inputs.

With the exception of one output, the approximating functions perform well. Known sensitivities, particularly the importance of diapycnal (vertical) eddy diffusivity and wind stress, are reproduced. The sensitivities of the model to two numerical constraints specific to the isopycnal parameterization, maximum allowable isopycnal slope and horizontal background eddy diffusivity, are explored. Isopycnal modelling issues, convection reduction and the Veronis effect, are examined and found to depend crucially on the isopycnal modelling constraints.

1. Introduction

The isopycnal version of the Bryan-Cox ocean general circulation model has been used by several investigators (Cummins *et al.,* 1990; Gerdes *et al.,* 1991; Gough, 1991; England, 1992; Manabe *et al.,* 1991; Gough and Lin, 1992). A comprehensive

1. Physical Sciences Division, Scarborough College, University of Toronto, 1265 Military Trail, Scarborough, Ontario, Canada, M1C 1A4.
2. Department of Statistics and Actuarial Science, University of Waterloo, Waterloo, Ontario, Canada, N2L 3G1.

examination of the parameter space of this model, though, has not been reported. The 'isopycnal' nature of the model refers to the method in which sub-grid scale processes are parameterized. Traditionally, (Bryan, 1969; Cox, 1984) these processes are aligned to the coordinate surfaces which are geopotentials and the perpendiculars to geopotentials (horizontal and vertical). It has been suggested in the literature that mixing processes would be better modelled along isopycnals (constant density surfaces) and diapycnals (perpendiculars to constant density surfaces) (Veronis, 1975; Sarmiento, 1983; McDougall and Church, 1985). In this model the isopycnal surfaces are locally referenced producing true "neutral" surfaces (McDougall, 1987).

Montgomery (1940) and others suggested that large-scale oceanic flow may mix preferentially along isopycnals. For example, it was noted from observational data that there were no salinity maxima on isopycnal surfaces, except at the intersections of these surfaces with the wind-driven mixed layer and lateral boundaries. Broecker and Peng (1982) examined the ^{3}He distributions in the Pacific, and found that this tracer appeared to spread along isopycnals into the other ocean basins.

Other evidence to support isopycnal mixing is less direct. It has been proposed to explain deficiencies in modelling studies. Veronis (1975) first noted the appearance of anomalous heat, and therefore density fluxes near the western boundary in Holland's (1971) model simulation of the general circulation of the North Atlantic. He argued that lateral mixing in that region produced a large diapycnal flux. As the lateral boundaries are thermally insulated, this heat (or density perturbation) could only be balanced by an increase in the upwelling of cold water. This enhanced upwelling, in turn, needed to be compensated by increased downwelling elsewhere, as reflected in Holland's results. This is contrary to the classical view (Stommel, 1958) of weak, widespread upwelling in the ocean interior. Veronis further suggested that the use of an isopycnal mixing parameterization would eliminate this problem, as the removal of a large diapycnal flux in the western boundary would no longer result in enhanced upwelling. McDougall and Church (1986) also invoked isopycnal mixing to explain large density fluxes found in the same region in the results of Cox and Bryan (1984). Note that both Holland (1971) and Cox and Bryan (1984) used a large horizontal eddy diffusivity. Veronis (1975) reported that the use of a lower diffusivity mitigated the downwelling problem. Gough (1991) found that the 'Veronis effect' was lower for the isopycnal model. This reduction, though, was limited by a horizontal background eddy diffusivity required for numerical stability. He also found that the isopycnal model produced a shallower thermocline, weaker thermohaline circulation, and a dramatic reduction in the number of convection points. This reduction appears to be only partially compensated by an increase in vertical eddy diffusivity due to sloping isopycnals in convective regions.

In this study the isopycnal model is examined over a broader range of parameter

values than was used in Gough (1991). One goal is to cover this broader range of physically reasonable values in a computationally efficient manner. Statistical techniques are used both to design the experiments and evaluate the output. The basic idea is to build a statistical approximation for each output of interest (kinetic energy density, etc.) as a function of several inputs considered (diffusivities, etc.). Model sensitivities can then be quickly evaluated via the approximating functions, which are more computationally efficient to produce. In contrast, the ocean general circulation model is expensive to evaluate, so we construct the approximations using only a limited number of runs, chosen according to a statistical experimental design.

In Section 2 the model and experimental design are described. The methods for building the approximating functions, their use to estimate sensitivities, and the results are reported and discussed in Section 3. Finally, in Section 4 the conclusions are presented.

2. Model description and experimental design

a. Model

i. Governing equations. The model used in this work is the widely distributed Bryan-Cox ocean general circulation model. It is based on the pioneering work of Bryan (1969). A detailed description of the model can be found elsewhere (Cox, 1984). The notation used is standard and is listed in the Appendix.

In this study, homogenization of temperature and salinity through intense vertical diffusion occurs when vertical instability is detected (Cox, 1984). Marotzke (1991) has found that this method effectively removes static instability. A value of $A_v = 10^4$ cm^2/s is used for convective adjustment which is four orders of magnitude larger than the nominal vertical eddy diffusivity value of $A_v = 1$ cm^2/s (Killworth, 1989).

ii. Boundary conditions. In this model the only source of heat (temperature) and salinity forcing is at the upper surface. Therefore, at the side walls and bottom, a no-flux condition is imposed.

For the vertical side walls there is a no-slip ($u, v = 0$) condition. At the bottom boundary, the flow is constrained to be parallel to the bottom topography, $w = 0$, in the case of this model with a flat bottom. The condition on u and v is determined by the imposed bottom friction,

$$\tau_\lambda = \rho_o C_D (u^2 + v^2)(u\cos\alpha - v\sin\alpha) \tag{1}$$

$$\tau_\phi = \rho_o C_D (u^2 + v^2)(u\sin\alpha - v\cos\alpha) \tag{2}$$

where C_D, the drag coefficient, is 1.3×10^{-3} and α, the turning angle, is $-10°$ for this study. For the vertical velocity, the rigid lid approximation is used ($w = 0$ at $z = 0$).

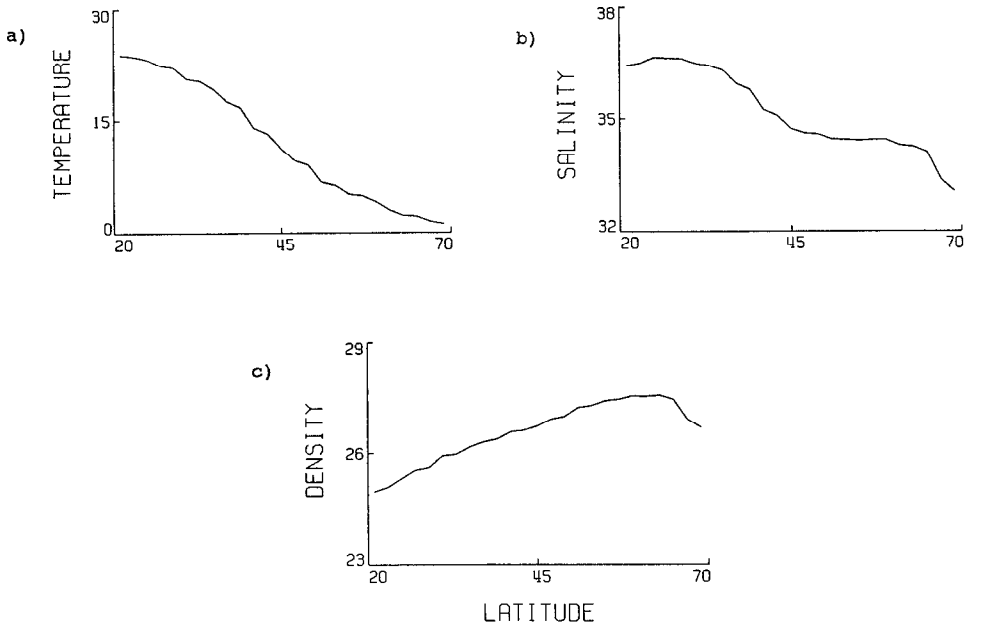

Figure 1. Surface restoring values of (a) temperature, (b) salinity, and (c) density. The temperature is in units of Celsius, the salinity in parts per thousand, and the density in sigma representation ($\sigma = \rho - 1000.0\ kg/m^3$).

The horizontal momentum, at the upper surface, is forced by the atmospheric winds. This is accomplished by using idealized wind stresses (τ_λ, τ_ϕ) given by the following analytic representation,

$$\tau_\phi = 0.2 - 0.8\sin(6\phi) \tag{3}$$

$$\tau_\lambda = 0.0 \tag{4}$$

with the stress in units of dynes/cm^2. This particular choice is designed to give a two gyre circulation in the North Atlantic, the approximate region of the model domain.

In this work restoring boundary conditions are used for both temperature and salinity (Haney, 1971). Zonally and temporally averaged (annual mean) restoring temperatures (T^*) and salinities (S^*) are taken from the Levitus (1982) climatological atlas for the ocean. These values are presented in Figure 1 with the implied restoring densities. The diffusion constant, D, is a constant, spatially and temporally, and corresponds to a restoring timescale of 50 days for a 50 m upper layer.

iii. Parameterization of sub-grid scale processes. In the momentum equation, the sub-grid scale processes are parameterized using eddy viscosities. Due to the predominantly horizontal flow, the horizontal eddy viscosity, $A_{MH} \equiv 10^9$ cm^2/s, which is much larger than the vertical eddy viscosity, $A_{MV} \equiv 1.0$ cm^2/s. Bryan (1987)

showed that there is much less sensitivity to the parameterization used in the momentum equations than there is in the temperature and salinity equations. In particular, Bryan found that the depth of the thermocline, the meridional and zonal mass transports, and the northward heat transport all depended crucially on the value chosen for the vertical eddy diffusivity.

As discussed in the Introduction the parameterization of the sub-grid scale eddy processes could be done using isopycnal and diapycnal mixing rather than the traditional vertical and horizontal (geopotential) coordinate system. Redi (1982) derived a coordinate transformation which represents isopycnal mixing in a model based on a geopotential coordinate system. Cox (1987) produced the necessary code to implement this mixing in the Bryan-Cox model.

Two assumptions are made to simplify the Redi tensor (Cox, 1987). Since mixing along isopycnals greatly exceeds mixing across isopycnals we assume that $\epsilon \ll 1$; the isopycnal slope is usually small $\delta < 10^{-2} \ll 1$. Here, $\epsilon = A_D/A_I$, the ratio of the diapycnal to isopycnal eddy diffusivity and $\delta = (\rho_x^2 + \rho_y^2)^{1/2}/\rho_z$. This results in a simplified tensor where the indices x, y and z denote the partial differentiation with respect to zonal, meridional and vertical directions respectively,

$$K = A_I \begin{vmatrix} 1 & \dfrac{-\rho_x\rho_y}{\rho_z^2} & -\dfrac{\rho_x}{\rho_z} \\ \dfrac{-\rho_x\rho_y}{\rho_z^2} & 1 & -\dfrac{\rho_y}{\rho_z} \\ -\dfrac{\rho_x}{\rho_z} & -\dfrac{\rho_y}{\rho_z} & \epsilon + \delta^2 \end{vmatrix} \tag{5}$$

b. Inputs and outputs

Seven input parameters are examined, the diapycnal and isopycnal eddy diffusivities (A_D, A_I), the vertical and horizontal eddy viscosities (A_{MV}, A_{MH}), the horizontal background eddy diffusivity (A_B), the maximum allowable isopycnal slope (δ_m), and the peak value of the wind stress (τ_m).

The horizontal background eddy diffusivity and maximum allowable isopycnal slope are numerical constraints arising from the use of the isopycnal mixing parameterization (Cox, 1987). The peak wind stress value is varied by changing the coefficient of the sine term in Eq. 3. Table 1 contains the range of values for the seven parameters. These ranges should be kept in mind when interpreting the results: sensitivity with respect to a parameter would tend to increase if a wider range is chosen.

The model flow is represented by six scalar outputs. They are the basin averaged kinetic energy density (KE), the peak value of the meridional streamfunction (MMT), the peak value of the northward heat transport (NHT), the bottom

Table 1. Input parameter range.

	Parameter Range
Diapycnal eddy diffusivity, A_D	0.5–10.0 cm^2/s
Isopycnal eddy diffusivity, A_I	$(0.5–5.0) \times 10^7$ cm^2/s
Vertical eddy viscosity, A_{MV}	0.5–20.0 cm^2/s
Horizontal eddy viscosity, A_{MH}	$(0.5–3.0) \times 10^9$ cm^2/s
Horizontal background eddy diffusivity, A_B	$(0.1–2.0) \times 10^7$ cm^2/s
Maximum allowable isopycnal slope, δ_m	0.001–0.1
Peak wind stress, τ_m	0.0–1.8 dynes/cm^2/s

temperature at 63N, 30W (TEMP), the number of convecting points (CONV) and the number of downwelling points (DOWN). The first three are familiar measures of the model flow. The bottom temperature at 63N, 30W is a measure of the deep water formation in the northern convective region. The number of convecting points was shown to substantially reduce with the use of an isopycnal mixing parameterization (Gough, 1991). Enhanced vertical eddy diffusivity due to the parameterization effectively replaced convection. The number of downwelling points is a measure of the Veronis effect (Veronis, 1975).

c. Experimental design

A total of 51 experiments (Table 2) are performed to explore the parameter space defined by the ranges in Table 1. To insure the efficient use of computing resources statistical techniques are employed to design the experiments and evaluate the model output.

To sample the seven parameter input space uniformly, a Latin hypercube experimental design (McKay *et al.,* 1979) is used. These designs were proposed for deterministic numerical experiments (i.e., without random error, as here).

To construct a Latin hypercube for n model runs, each parameter's range is represented by an equally-spaced grid of n values. Thus the range is fully explored. Available computer resources allow for an initial 25 to 30 runs of the model to be completed in a reasonable time (two weeks) on a series of workstations. Taking n = 26 runs gives spacing of $1/25$ of each parameter's range. Thus, it is seen in Table 2 that A_D, for example takes values of 0.5, 0.88, 1.26, . . . , 10 cm^2/s in the first 26 rows though not in order. Because the maximum allowable isopycnal slope has a range covering two orders of magnitude, we actually work with the logarithm of this parameter. Therefore, the log (δ_m) values are equally spaced. Similarly, in subsequent statistical analysis we will work with log (δ_m) rather than δ_m.

For a completely random Latin hypercube, the 26 values for each parameter would be in a random order, this ordering being statistically independent of those for other parameters. Combining, for example, the 26 A_D values with the 26 A_I values at random in this way hopefully fills out the two-dimensional A_D/A_I space, representing all combinations of these two parameters. There is no guarantee, however, that

Table 2. List of experiments. Symbols according to the Appendix.

Case	A_D cm^2/s	A_I $10^7\ cm^2/s$	A_{MV} cm^2/s	A_{MH} $10^9\ cm^2/s$	A_B $10^7\ cm^2/s$	δ_m	τ_m dynes/cm^2/s
1	0.500	1.400	17.66	0.700	2.000	0.0692	1.080
2	6.960	2.840	9.080	1.400	1.696	0.0331	1.800
3	5.440	3.380	16.10	1.100	0.100	0.0158	0.576
4	9.620	1.760	5.960	2.700	0.556	0.0052	0.216
5	0.880	5.000	12.20	1.300	0.860	0.0010	1.224
6	6.580	1.040	2.840	1.700	1.240	0.0063	0.504
7	4.300	4.100	19.22	1.900	1.392	0.0275	0.000
8	2.020	3.020	5.180	2.200	0.708	0.0479	0.792
9	2.400	0.860	9.860	1.000	0.252	0.0132	1.296
10	6.200	4.280	12.98	0.500	0.176	0.0025	0.144
11	2.780	1.580	4.400	2.400	0.784	0.0044	1.368
12	7.720	4.460	10.64	3.000	1.088	0.0036	1.728
13	1.640	3.560	11.42	2.900	1.924	0.0021	1.008
14	8.860	1.220	13.76	1.500	1.848	0.0110	1.152
15	9.240	4.640	2.060	1.600	1.316	0.0575	0.432
16	5.820	2.660	15.32	0.800	1.164	0.0229	0.720
17	4.680	0.500	16.88	2.600	1.544	0.0191	0.072
18	7.340	3.920	8.300	2.800	0.936	0.1000	0.288
19	5.060	1.940	3.620	1.200	0.404	0.0832	1.656
20	3.920	3.740	14.54	2.100	1.012	0.0030	0.936
21	8.480	4.820	7.520	0.900	1.468	0.0012	1.584
22	1.260	2.120	1.280	1.800	0.632	0.0017	0.360
23	10.00	0.680	20.00	2.300	0.328	0.0091	1.440
24	8.100	2.300	6.740	0.600	1.772	0.0076	0.648
25	3.160	3.200	18.44	2.500	0.480	0.0398	1.512
26	3.540	2.480	0.500	2.000	1.620	0.0014	0.864
27	10.00	4.990	0.576	2.365	0.100	0.1000	1.800
28	2.054	0.503	19.96	0.507	1.031	0.0993	0.365
29	9.417	3.653	2.808	0.928	0.383	0.0704	0.003
30	5.176	1.526	20.00	3.000	0.103	0.0010	0.585
31	10.00	4.490	15.66	1.189	2.000	0.0426	0.440
32	0.501	1.856	0.549	2.973	1.360	0.0117	1.491
33	5.859	0.555	2.095	2.209	1.991	0.0011	1.420
34	0.506	2.357	15.70	1.515	0.104	0.0044	0.002
35	4.747	3.311	2.431	0.500	0.825	0.0119	1.800
36	5.067	4.462	8.021	1.600	0.501	0.0998	0.893
37	9.856	0.789	19.19	1.485	0.707	0.0025	1.662
38	4.500	5.000	15.27	2.999	1.759	0.0654	0.246
39	3.483	4.999	4.751	0.500	0.344	0.0219	1.080
40	1.691	4.086	15.19	2.663	0.335	0.0010	1.796
41	7.652	0.942	0.517	0.776	0.911	0.0440	0.124
42	7.989	0.505	4.107	2.780	0.129	0.0713	0.846
43	10.00	2.882	17.46	0.501	1.304	0.0015	1.279
44	8.837	2.096	12.13	2.088	0.496	0.0206	1.795
45	0.591	4.435	19.99	1.012	1.637	0.0061	0.739
46	1.218	3.185	6.600	2.995	1.625	0.0998	0.000
47	9.158	4.942	9.151	2.579	1.052	0.0019	0.594
48	3.182	3.956	7.989	2.203	0.100	0.0106	0.316
49	3.307	0.784	11.89	1.164	1.402	0.0921	0.623
50	2.729	4.976	19.82	1.742	1.997	0.0034	0.097
51	7.315	3.266	19.99	1.213	0.213	0.0015	1.096

random ordering will give good two- and higher dimension properties. In particular, two parameters might be highly correlated with each other by chance, making it difficult to separate their effects on the outputs. Iman and Conover (1982) described how to transform a starting, completely random Latin hypercube into one with better correlation properties. By iterating their method, an obvious adaptation of their algorithm, successive improvements converge to a Latin hypercube with very good correlation properties. The design in the first 26 rows of Table 2 has correlations less than 0.04 for all possible pairs of parameters.

Of the 26 runs, five prove unstable (refer to Section 3a). Following the method to be outlined in Section 3b, approximating functions are fitted and assessed for accuracy for each output using the 21 successful runs. For now, though, we just note that these functions do not yield sufficient accuracy, and a further 25 model runs are made.

These additional runs are chosen to augment the 21 successful runs from the first experimental design. To improve the coverage of the input space, the 25 new runs are selected to fill in sparse subregions. Specifically, the new input points are chosen to be distant from the successful first-stage design points and from each other. These additional runs are given in rows 27–51 of Table 2.

Of the 25 new runs, 10 are unstable. The 15 successful runs, together with the 21 from the first-stage design, give a total of 36 stable cases. All output data appear in Table 3.

3. Results and discussion

The 51 experiments are integrated for 1500 years. The integrations are begun at rest. A split time step method is used (Bryan, 1984); the temperature and salinity equations use a one day time step whereas the momentum equations use a 30 minute time step. Due to the restoring density field (Fig. 1) a density driven (thermohaline) circulation is set up. There is intense downwelling in the north where the restoring density peaks and gradual upwelling in much of the rest of the domain. A wind driven Ekman circulation is also generated in the upper ocean. The strength of this circulation is dependent on the magnitude of the peak wind stress.

The results are divided into four sections. The first is an examination of the cases that did not achieve a stable solution after 1500 years. In the second section the performance of a statistical model of the ocean general circulation model based on the model output is presented. In the third section, the dependence of output scalars on the input parameters is explored using the statistical model. Finally, in the fourth section, an overall assessment of the input parameters is made.

a. Unstable cases

Fifteen of the 51 cases are considered unstable. Cases 3, 15, 18, 19, 27, 29, 31, 36, 38, and 46 exhibit explosive behavior and the integrations are terminated. Cases 23,

Table 3. Model output.

Case	KE ergs/cm^3	MMT Sv	NHT PW	CONV	TEMP °C	DOWN
1	0.450	10.30	0.231	19	3.96	3038
2	1.423	24.83	0.731	65	5.02	2534
4	0.934	28.42	0.764	388	4.38	2258
5	0.589	8.88	0.265	424	3.73	2299
6	0.671	24.37	0.638	559	4.52	2532
7	0.299	19.38	0.494	5	4.06	2456
8	0.385	12.06	0.350	4	3.68	2031
9	1.104	11.78	0.437	147	3.55	2034
10	0.958	20.10	0.612	235	4.17	2219
11	0.723	13.77	0.462	422	3.97	2211
12	1.182	23.54	0.784	389	4.79	2479
13	0.293	11.34	0.310	375	3.95	2662
14	1.070	28.51	0.776	519	5.07	2563
16	0.883	22.63	0.619	52	4.46	2406
17	0.310	21.04	0.505	354	4.30	2532
20	0.581	16.75	0.512	319	4.11	2438
21	1.489	25.04	0.784	855	5.47	2592
22	0.174	8.95	0.244	337	3.42	2259
24	0.975	28.60	0.715	404	4.81	2692
25	0.886	14.58	0.495	1	3.80	2120
26	0.444	16.40	0.467	665	4.44	2492
28	0.327	14.06	0.320	38	3.88	2256
30	0.579	16.45	0.579	948	4.33	2334
32	0.484	9.08	0.233	131	3.63	2511
33	0.829	22.79	0.627	1276	5.19	2536
35	2.166	22.25	0.580	161	4.63	2369
37	1.895	24.11	0.889	1237	5.39	2236
40	0.933	9.54	0.397	566	3.83	2343
41	1.023	26.81	0.661	53	4.41	2113
43	1.736	28.56	0.837	1012	5.59	2609
44	1.435	24.31	0.823	62	4.53	2328
45	0.230	8.12	0.190	82	3.56	2730
47	0.791	25.74	0.775	554	4.87	2679
49	0.441	17.42	0.437	38	4.24	2373
50	0.145	14.04	0.392	187	3.98	2814
51	1.309	18.18	0.765	702	4.87	2474

34, 42, and 48 have unconverged, oscillatory solutions by year 1500. Finally, 'negative diffusion' resulting in bottom water that is colder than the coldest restoring temperature has been detected in case 39 similar to that found by Gough (1991) and Gerdes *et al.* (1991). Negative diffusion is also detected in oscillatory cases 34 and 48, and unstable case 3.

Nine of the unstable cases can be attributed to a numerical constraint associated

with the use of the isopyncal mixing parameterization. Cox (1987) derived the following constraint on the maximum allowable isopycnal slope,

$$\delta_m < \left(\frac{\Delta a \Delta z}{4 A_I \Delta t}\right)^{1/2} \tag{6}$$

where Δa, Δz, Δt, and A_I refer to the horizontal grid spacing, vertical grid spacing, timestep, and isopycnal eddy diffusivity, respectively. Choosing the smallest horizontal grid spacing (at the most northerly latitudes) and smallest vertical level depth, it is found that the maximum allowable isopycnal slopes selected for cases 15, 18, 19, 27, 29, 31, 36, 38, and 46 do not satisfy this criteria, all of which displayed explosive behavior.

The remaining unstable cases are characterized by a low horizontal background eddy diffusivity (cases 3, 34, and 48) or low combined horizontal background and isopycnal eddy diffusivity (cases 23 and 42). Cox (1987) indicated that it may be necessary to include a horizontal background eddy diffusivity to suppress the growth of a computational mode. Case 30 which was stable had a horizontal background eddy diffusivity of 1.03×10^6 cm^2/s, less than that of case 34. The stability of this case, though, is likely the result of the very shallow maximum allowable isopycnal slope (0.001, an order of magnitude smaller than cases 3, 34, and 48), and a sufficiently large isopycnal eddy diffusivity (1.526×10^7 cm^2/s). Bryan *et al.* (1975) reported that the horizontal eddy diffusivity needed to be sufficiently large to suppress the computational mode which may explain the behavior of cases 23 and 42. Theirs are the lowest combined values of the horizontal background and isopycnal eddy diffusivity.

The 'negative diffusion' found in cases 3, 34, 39, and 48 is associated with three input parameters; large isopycnal eddy diffusivity, low horizontal background eddy diffusivity, and steep maximum allowable isopycnal slope. Other cases with a large isopycnal to horizontal background eddy diffusivity ratio which do not produce negative diffusion have a shallow maximum allowable isopycnal slope (e.g., cases 10, 30, and 51). Gerdes *et al.* (1991) attributed the negative diffusion to the use of one-sided differences at boundaries in regions that were topographically isolated from advection. A definitive threshold for negative diffusion as a function of these three inputs has not been obtained from the results.

b. Statistical modelling

Using the 36 stable cases listed in Table 3, statistical approximating functions are constructed for each output as a function of the seven inputs. We follow the methodology described in Sacks *et al.* (1989a,b) and Welch *et al.* (1992). Bowman *et al.* (1993) applied these methods to an atmospheric model. Details can be found in these papers; here we outline the main ideas.

Let $\mathbf{x} = (x_1, \ldots, x_7)$ denote the vector of input parameters, and let y denote one of the outputs (each of the six outputs of interest is dealt with in turn). We treat $y(\mathbf{x})$ as a

realization of a stochastic process,

$$Y(\mathbf{x}) = \beta_o + Z(\mathbf{x}) \tag{7}$$

where β_0 is an unknown constant and $Z(\mathbf{x})$ is a random function with mean zero and correlation function $R(\mathbf{w}, \mathbf{x})$ between the two Z values at input $\mathbf{w}$ and $\mathbf{x}$. Note that a realization of a stochastic process is nonrandom, like the deterministic computer model here, but embedding the function in a stochastic structure gives a basis for constructing a predictor.

Central to this model is the correlation function $R(\mathbf{w}, \mathbf{x})$. Sacks *et al.* (1989b) found,

$$R(\mathbf{w}, \mathbf{x}) = \Pi_j e^{(-\theta_j |w_j - x_j|^{p_j})} \tag{8}$$

to be useful in a number of applications, where $\theta_j \geq 0$ and $0 < p_j \leq 2$ are parameters to be estimated. If we further assume that the stochastic process in Eq. 7 is Gaussian, the optimization of these parameters by maximum likelihood to tune the model to the data is straightforward. Qualitatively, this correlation structure implies that two input vectors $\mathbf{w}$ and $\mathbf{x}$ that are close together in the input space should give rise to values of the output function that are highly correlated (i.e., similar), as would be expected if the function is smooth. Conversely, $\mathbf{w}$ and $\mathbf{x}$ when remote from each other lead to two output values with low correlation (i.e., unrelated).

Thus, we first tune the statistical model to the data: β_0 in Eq. 7, $\theta_1, \ldots, \theta_7$ in Eq. 8, and $p_1, \ldots, p_7$ in Eq. 8 are estimated by maximum likelihood. Then, a best linear unbiased predictor,

$$\hat{y}(\mathbf{x}) = \hat{\beta}_o + \mathbf{r}'(\mathbf{x})\, \mathbf{R}_D^{-1}\, (\mathbf{y} - \hat{\beta}_o \mathbf{1}) \tag{9}$$

is computed where $\mathbf{r}(\mathbf{x})$ is an $n \times 1$ vector of correlations with element i given by $R(\mathbf{d}_i, \mathbf{x})$ in Eq. 8 and $\mathbf{d}_i$ is the vector of input parameters for run i of the design of the numerical experiments; $\mathrm{R_D}$ is an $n \times n$ matrix of correlations with element i, j given by $R(\mathbf{d}_i, \mathbf{d}_j)$ in Eq. 8; $\mathbf{1}$ denotes an $n \times 1$ vector of 1's; $\mathbf{y}$ is the $n \times 1$ vector of output values from the numerical model for a particular response; and $\hat{\beta}_0$ is the generalized least squares estimator of β_0 given by $\hat{\beta}_0 = \mathbf{1}'\mathbf{R}_D^{-1}\, \mathbf{y}/\mathbf{1}'\mathbf{R}_D^{-1}\, \mathbf{1}$. This predictor is more flexible than, say, a low-order polynomial fit, and has been found to yield more accurate predictions in various applications.

To assess the fidelity of the statistical model, predicted values using the tuned model are plotted against the actual model output in Figure 2. The ith value of the response, y_i is predicted using all data except y_i, a method of prediction-accuracy assessment known as cross validation. There is reasonable agreement between predicted and actual values for the first five outputs. In Figure 2a for the large values of kinetic energy the statistical model underpredicts the value. Similarly large values of convection are not as well predicted as lower values are. The overturning streamfunction, the northward heat transport, and the bottom temperature are all

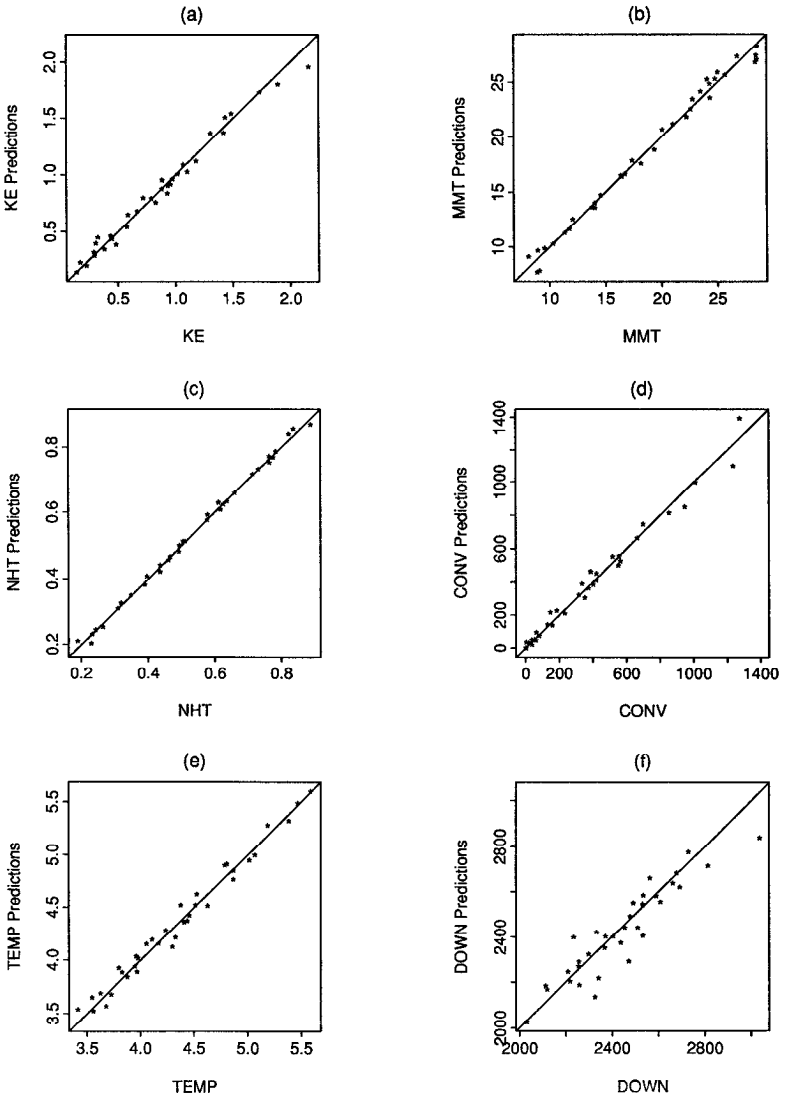

Figure 2. Cross validation predictions against values in the numerical experiments for the six outputs.

well predicted. In Figure 2f, the modelling of downwelling points is seen to be less accurate, however, and for this output our results should be treated with caution. This means the ocean general circulation model is reasonably predictable, and our subsequent results and inferences about sensitivities appear to be based on reliable approximations.

c. Dependencies of output on input

The predictor, Eq. 9, "explains" the dependency of an output y on multi-dimensional inputs $x_1, \ldots, x_7$. To assess sensitivities, however, we want to determine the effect of individual x variables on y. To estimate the effect of x_j integrate out all other inputs from the predictor $\hat{y}$:

$$\hat{\mu}_j(x_j) = \frac{\int \hat{y}(x_1, \ldots, x_7)\, \Pi_{i \neq j}\, dx_i}{\Pi_{i \neq j}\, (b_i - a_i)} \tag{10}$$

where (a_i, b_i) is the range of values for x_i and $\Pi_{i \neq j}$ denotes the product over all i and not equal to j.

Similarly, the dependence on the joint effect of x_j and x_k can be estimated by integrating out all variables except these two,

$$\hat{\mu}_{jk}(x_j, x_k) = \frac{\int \hat{y}(x_1, \ldots, x_7)\, \Pi_{i \neq j,k} dx_i}{\Pi_{i \neq j,k}(b_i - a_i)} \tag{11}$$

and so on for higher order effects. To assess the importance of the joint effect over and above that explained by $\mu_j(x_j)$ and $\mu_k(x_k)$ we consider the estimated interaction effect,

$$\hat{\mu}_{jk}(x_j, x_k) - \hat{\mu}_j(x_j) - \hat{\mu}_k(x_k) + \hat{\mu}_O \tag{12}$$

where

$$\hat{\mu}_O = \frac{\int \hat{y}(x_1, \ldots, x_7) \Pi_{i=1}^{7}\, dx_i}{\Pi_{i=1}^{7}\, (b_i - a_i)} \tag{13}$$

is the overall estimated average value of the response y. If this interaction effect is small, x_j and x_k have approximately additive effects, it is sufficient to look at the separate $\hat{\mu}_j(x_j)$ and $\hat{\mu}_k(x_k)$ effects, and $\hat{\mu}_{jk}(x_j, x_k)$ need not be inspected. This turns out to be the case for all outputs except convection (CONV). If a $\hat{\mu}_{jk}(x_j, x_k)$ term is important, however, then it is difficult to isolate the effects of x_j or x_k individually, and we have to assess sensitivity with respect to both parameters jointly.

i Kinetic energy density. Figure 3 shows the 'main effects,' $\hat{\mu}_j(x_j)$ plotted against x_j for the x variables estimated to have important effects on KE. Thus, the plot labelled KE (DIA) gives the estimated effect of diapycnal eddy diffusivity on the kinetic energy. Unimportant x variables just give fairly horizontal plots; hence their omission.

Four factors are identified as important in determining the kinetic energy. Kinetic energy increases with diapycnal eddy diffusivity and peak wind (WIND). It decreases with horizontal eddy viscosity (HORVIS) and horizontal background eddy diffusivity

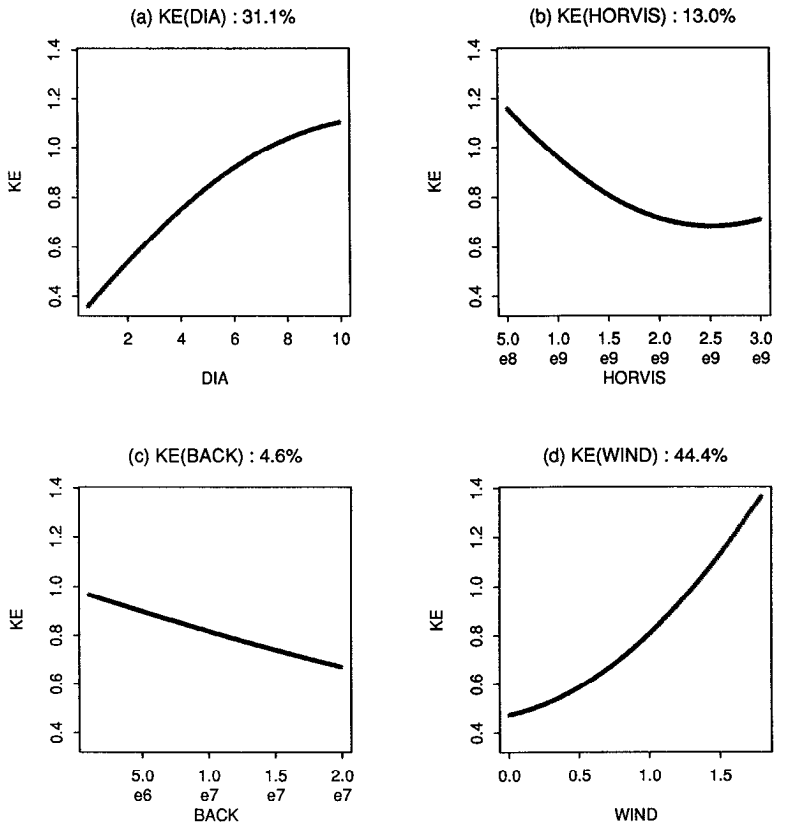

Figure 3. Kinetic energy density (KE) main effects, (a) diapycnal eddy diffusivity (DIA), (b) horizontal eddy viscosity (HORVIS), (c) horizontal background eddy diffusivity (BACK), and (d) peak wind stress (WIND).

(BACK). The percentages attached to each plot give a quantitative assessment of the relative sensitivities. For example, of the total variability in kinetic energy due to varying all seven inputs over the ranges investigated, peak wind alone accounts for an estimated 44.4%.

These dependencies are as expected and illustrate the two main circulations, wind driven (Ekman) and buoyancy driven (thermohaline). Bryan (1987) found that increasing the vertical eddy diffusivity (the equivalent to the diapycnal eddy diffusivity) increased the overturning streamfunction, a measure of the thermohaline circulation. Increasing the peak wind stress increases the Ekman circulation, thereby increasing the kinetic energy. Both the horizontal background eddy diffusivity and the horizontal eddy viscosity act to dampen the flow (particularly the gyre component) and thus cause a reduction in the kinetic energy. The horizontal eddy viscosity acts directly on the flow whereas the horizontal background eddy diffusivity mixes

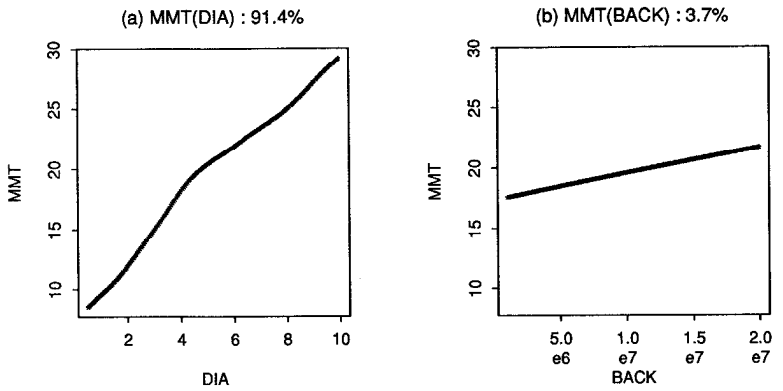

Figure 4. Meridional overturning streamfunction (MMT) main effects, (a) diapycnal eddy diffusivity (DIA), and (b) horizontal background eddy diffusivity (BACK).

temperature and salinity along horizontal surfaces causing diapycnal flow which smooths the density field. This results, through geostrophy, to a lower kinetic energy.

ii. Meridional overturning streamfunction. There is one dominant component and one component of secondary importance in determining the peak value of the overturning streamfunction (MMT) (Fig. 4). As noted above this value is a measure of the buoyancy driven thermohaline circulation. The dominant effect is the increase of the streamfunction with the diapycnal eddy diffusivity, a result consistent with Bryan (1987). The estimated increase of the overturning streamfunction with horizontal background eddy diffusivity is marginal (only 3.7% of the total variability) and may be spurious. It should also be noted that the surface buoyancy forcing which has remained constant for these experiments plays a major role in determining the nature and strength of the overturning streamfunction (Bryan, 1987).

iii. Northward heat transport. The northward heat transport is known to depend upon both the buoyancy and wind driven circulations. From Figure 5 we see that the heat transport depends strongly on the diapycnal eddy diffusivity (98.2%). As noted in the previous section, increased diapycnal eddy diffusivity increases the overturning streamfunction of the thermohaline circulation which results in a stronger heat transport. The increase of the peak wind intensifies the wind driven Ekman circulation also resulting in a stronger northward heat transport but this effect appears to be marginal (2.7% of the total variability).

iv. Convection. There are two important inputs for the number of convection points: maximum allowable isopycnal slope (72.7%) and isopycnal eddy diffusivity (10.3%) (Fig. 6), with horizontal background eddy diffusivity having a marginal effect (2.6%). For this output, however, we look to higher order effects: the interaction term,

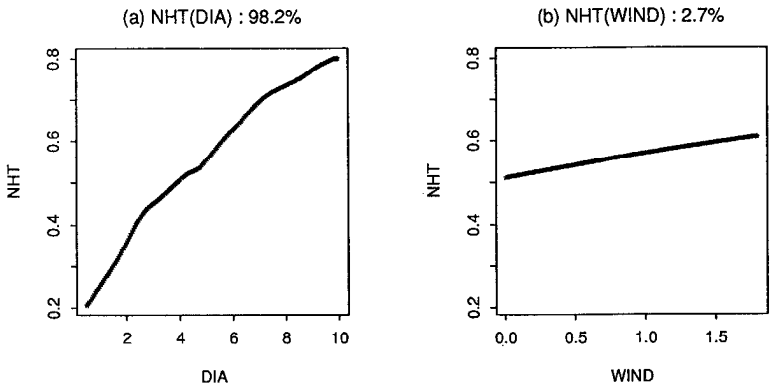

Figure 5. Northward heat transport (NHT) main effects, (a) diapycnal eddy diffusivity (DIA), and (b) peak wind stress (WIND).

Eq. 12, for the nonadditive effect of maximum allowable isopycnal slope (MAXSLP) and diapycnal eddy diffusivity (DIA) accounts for another 7.9% of the variability. In addition to the interaction effect, the main effects of diapycnal eddy diffusivity and maximum allowable slope are 2.4% and 72.7% respectively making a total of 83.1% that these two parameters jointly account for in the number of convection points. Figure 7 is a contour plot of the $\mu_{jk}(x_j, x_k)$ joint effect (Eq. 11) of these two parameters on CONV. It shows that the maximum allowable isopycnal slope has a larger effect on CONV when diapycnal eddy diffusivity is large. Thus, diapycnal eddy diffusivity, while having a negligible main effect, plays an important role in modifying the effect of the maximum allowable isopycnal slope.

The maximum allowable isopycnal slope dependency is explainable in terms of cross isopycnal mixing. With a low maximum allowable isopycnal slope, mixing is constrained to slopes less than the actual slope. This increases the diapycnal (cross isopycnal) flow and induces convection (Gough, 1991). As the maximum allowable isopycnal slope increases there is less diapycnal flux and, hence, less convection.

These results indicate that increasing the isopycnal eddy diffusivity also reduces the number of convection points. The reasons for this are unclear. One possible explanation (T. McDougall, personal communication) is that the stronger isopycnal mixing results in cabbeling (McDougall, 1987). Cabbeling is the densification of sea-water due to the nonlinear equation of state. This densification may mitigate the required amount of convection for stability.

v. Bottom temperature. There are four inputs that are important in the determination of the bottom temperature (Fig. 8). These are the diapycnal eddy diffusivity (68.7%), the horizontal background eddy diffusivity (15.8%), the peak wind stress (7.3%), and the maximum allowable isopycnal slope (4.5%).

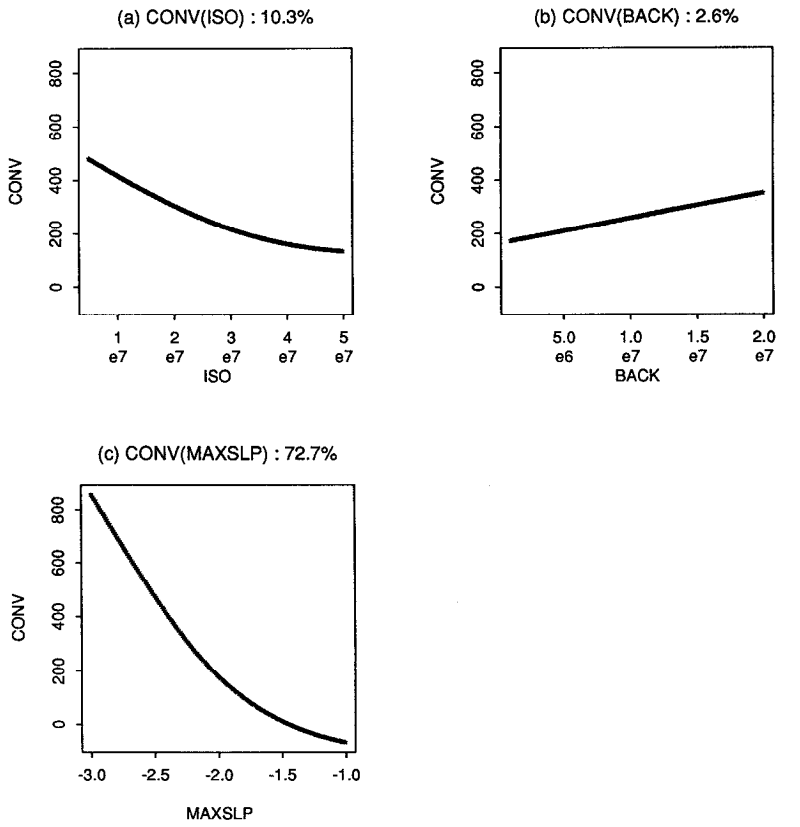

Figure 6. Convection (CONV) main effects, (a) isopycnal eddy diffusivity (ISO), (b) horizontal background eddy diffusivity (BACK), and (c) maximum allowable isopycnal slope (MAXSLP).

The source of cold bottom water is in the northern part of the domain through the surface restoring boundary condition on temperature. Water mass is transported via both the thermohaline and Ekman circulations to the bottom. If this combined circulation is intense then the downwelling waters are not cooled at the surface as much as those in a weaker flow. This mechanism explains the warmer temperature with increasing diapycnal eddy diffusivity. As noted above the overturning streamfunction, and hence the thermohaline circulation has a strong positive dependence on the diapycnal eddy diffusivity. The dependence on the peak wind is similarly explained as the Ekman circulation intensifies with increasing peak wind.

The warming of bottom waters due to increasing horizontal background eddy diffusivity is likely the result of the 'smoothing' effect of increased diffusivity. The bottom water at this location is typically the coldest water in the bottom of the basin. With increased horizontal eddy diffusivity there is a mitigation of temperature gradients producing muted extremes.

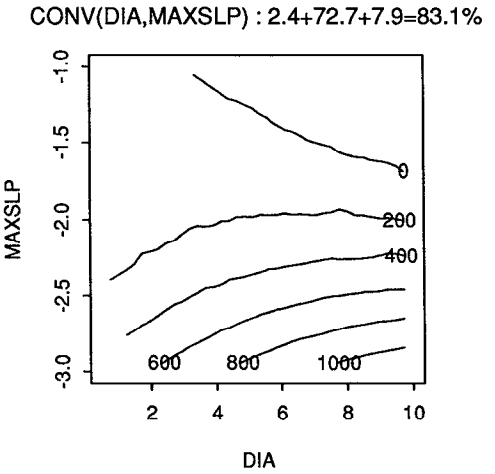

Figure 7. Joint effect of maximum allowable isopycnal slope (MAXSLP) and diapycnal eddy diffusivity (DIA) on the number of convection points (CONV).

The dependency on the maximum allowable isopycnal slope probably results from the location of the coldest bottom temperature. Low isopycnal slope due to the shallower sloping of the isopycnals (Gough, 1991) produces a cold extreme farther south than for higher slopes. Since the bottom temperature is taken at one location, the values are warmer for the shallower slopes. This effect, though, appears to be marginal.

vi. Downwelling. As the statistical approximating function is not as good for this output as it was for the previous five outputs, the statistical inferences need to treated with care.

The dominant effects are identified as horizontal background eddy diffusivity (59.8%), maximum allowable isopycnal slope (13.1%), and diapycnal eddy diffusivity (3.1%) (Fig. 9). The oscillatory nature of the diapycnal eddy diffusivity is unlikely to be correct and should be discounted. The dependencies upon the horizontal background eddy diffusivity and the maximum allowable isopycnal slope, though, are consistent with what is expected from the Veronis effect. As the horizontal background eddy diffusivity is increased there is more cross isopycnal flow in the western boundary. This causes stronger upwelling there; hence an increase in the number of interior downwelling points. Increasing the maximum allowable isopycnal slope reduces the cross isopycnal flow and thus there is a corresponding reduction in downwelling points.

d. Importance of inputs

This analysis has isolated the inputs which have the greatest impact on the selected model outputs. It is found that diapycnal eddy diffusivity plays an important role for

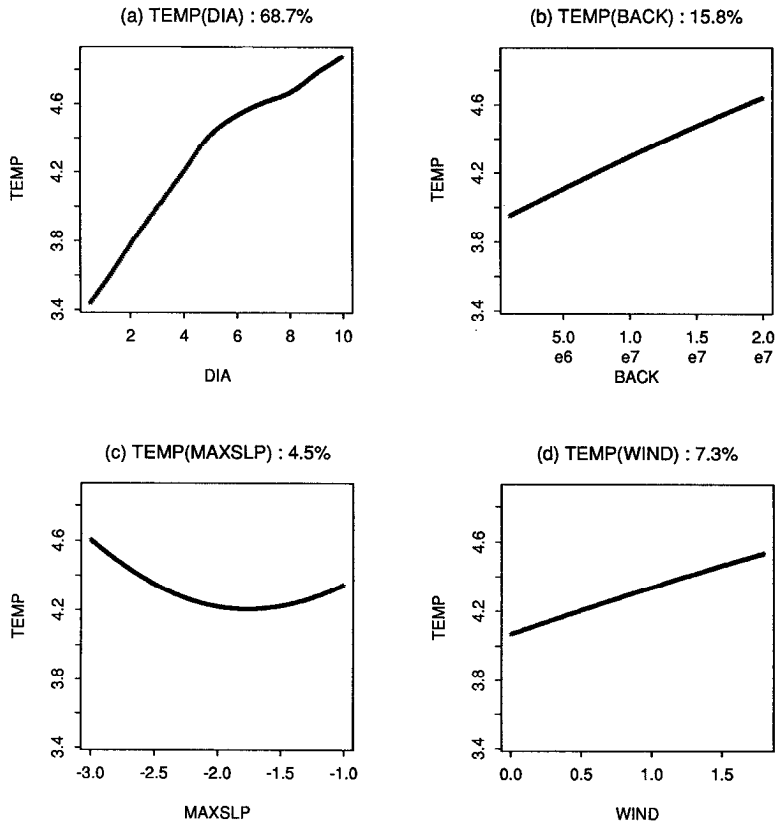

Figure 8. Bottom temperature (TEMP) main effects, (a) diapycnal eddy diffusivity (DIA), (b) horizontal background eddy diffusivity (BACK), (c) maximum allowable isopycnal slope (MAXSLP), and (d) peak wind stress (WIND).

the kinetic energy, meridional overturning streamfunction, the northward heat transport, and the bottom temperature. These are expected from the results of Bryan (1987) where vertical eddy diffusivity (his model's equivalent to diapycnal eddy diffusivity) was found to play a pivotal role. Diapycnal eddy diffusivity also has a higher order effect on the number of convection points. Isopycnal eddy diffusivity, in contrast, plays only a minor role in determining the number of convective points and does not significantly affect the other outputs.

The importance of the peak wind stress on the kinetic energy and bottom temperature is the result of a changed wind driven Ekman circulation, and is not surprising.

The horizontal eddy viscosity is important only for the kinetic energy where it acts to dampen the flow. This dampening affects the gyre (nonzonal) component of the flow (Gough, 1991). The vertical eddy viscosity does not play a significant role for any

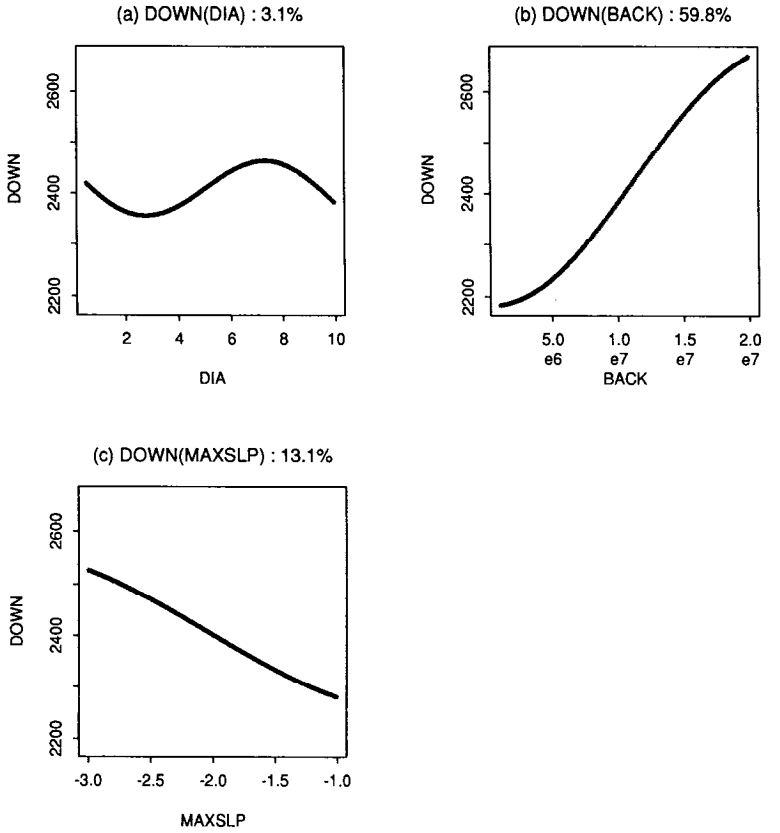

Figure 9. Downwelling (DOWN) main effects (a) diapycnal eddy diffusivity (DIA), (b) horizontal background eddy diffusivity (BACK), and (c) maximum allowable isopycnal slope (MAXSLP).

of the outputs. The value of this parameter is large enough for all experiments to prevent a Reynold's number violation (Weaver and Sarachik, 1990).

The maximum allowable isopycnal slope is an important input for three of the outputs: convection, bottom temperature, and number of downwelling points. It, along with the isopycnal eddy diffusivity, is crucial for the explanation of most of the unstable (explosive) cases detailed earlier (Section 3a). It was noted in Gough (1991) that the introduction of isopycnal mixing dramatically reduces the amount of convection. The maximum allowable isopycnal slope can be taken as a measure of how 'isopycnal' the model is; the strong dependence of the convection on the maximum allowable isopycnal slope confirms the earlier work.

The other additional parameter, the required horizontal background eddy diffusivity, is also shown to have important consequences. It plays a significant role in the bottom temperature and the number of downwelling points. Low values of this parameter are identified with explosive or oscillatory behavior in the experiments.

4. Conclusions

In this work we have shown that with the use of statistical techniques we have efficiently designed experiments to explore a wide range of the parameter space of the isopycnal version of the Bryan-Cox ocean general circulation model. Seven inputs are varied in 51 experiments. Fifteen of these cases are removed from the analysis due to explosive or oscillatory behavior and 'negative diffusion.' The explosive behavior is attributed to a numerical constraint violation for all but one of the explosive cases. Two of the oscillatory cases are the result of a combined low isopycnal and horizontal background eddy diffusivity. The remaining cases have a large isopycnal to horizontal background eddy diffusivity ratio resulting in 'negative diffusion' as identified in Gerdes *et al.* (1991).

In the analysis of the results six scalar outputs are used to characterize the flow. Statistical approximating functions of the ocean model are formed using the output. These functions, with one exception, show that the scalar output of the ocean general circulation model to be predictable. From this an analysis of the dependency of output on input is possible. Known sensitivities, such as the importance of the diapycnal eddy diffusivity and peak wind stress, are reproduced. The impact of two new constraints, introduced for the isopycnal mixing parameterization, horizontal background eddy diffusivity and the maximum allowable isopycnal slope, is shown. Several inputs, the vertical and horizontal eddy viscosity and isopycnal eddy diffusivity, play relatively minor roles for the ranges chosen for these experiments. The use of an experimental design which covered the parameter space multidimensionally, also allowed the exploration of complex two-parameter sensitivities. In this way, the role of diapycnal eddy diffusivity in modifying the effect of maximum allowable isopycnal slope on the number of convection points was discovered.

Two isopycnal modelling issues are explored by the convection and downwelling outputs. Gough (1991) found that isopycnal mixing dramatically reduced convective activity compared to a similar lateral mixing model. These results are confirmed in this study. The more 'isopycnal' the model (large maximum allowable isopycnal slope, low horizontal background eddy diffusivity) the lower the number of convective points. The number of downwelling points is introduced as a measure of the Veronis effect. Although the approximating function is not as good as those for the other outputs the dependency on the two 'isopycnal' constraints, maximum allowable isopycnal slope and horizontal background eddy diffusivity are as expected, i.e. the more 'isopycnal' the model the fewer the number of downwelling points.

There are several applications for this type of model design and statistical modelling. First, this methodology provides an efficient manner to design a series of experiments to explore the parameter range of a model with a number of tunable inputs. The isolation of the more sensitive inputs can be used in further experimental design as well as testing of various different parameterizations. Input parameters can also be tuned to produce a known result, such as specific values for the northward

heat transport or meridional overturning streamfunction. The methodology can also be expanded for use with vector inputs and outputs.

Another application is the production of output scalars for a given set of input parameters without actually running the full ocean general circulation model. This has application in simpler climate modelling where computing resources may be limited.

In this set of experiments the equilibrium response to variation of inputs is examined. Another aspect of interest, particularly in climate change modelling, is the sensitivity of inputs on the transient response of a model.

Acknowledgments. We would like to acknowledge the helpful comments of C. Lin, K. Dixon, R. Gerdes, A. Weaver, T. Hughes, T. McDougall, J. Sacks, and F. Zwiers. The work was done while the first author was a Visiting Fellow at the Canadian Climate Centre of Environment Canada in Downsview, Ontario, Canada. WJW was supported by NSERC of Canada, AFOSR and NSF through Grant NSF-DMS-9121554. Part of the work was done while WJW visited the National Institute of Statistical Sciences.

APPENDIX

α - Turning angle used in bottom drag
A_B - Horizontal background eddy diffusivity
A_D - Diapycnal eddy diffusivity
A_I - Isopycnal eddy diffusivity
A_{MH} - Horizontal eddy viscosity
A_{MV} - Vertical eddy viscosity
A_V - Vertical eddy diffusivity
C_D - Drag coefficient
δ - Isopycnal slope
δ_m - Maximum allowable isopycnal slope
D - Surface diffusion constant, restoring time of 50 days
ϕ - Latitude
λ - Longitude
ρ - Sea-water density
S^* - Restoring salinity
τ_λ - Wind stress
τ_ϕ - Wind stress
τ_m - Peak value of the wind stress
T^* - Restoring temperature
T^s - Sea-surface temperature
u - zonal velocity
v - meridional velocity
w - vertical velocity
CONV - number of convection points

DIA - diapycnal eddy diffusivity
DOWN - number of downwelling points
HORVIS - horizontal eddy viscosity
ISO - isopycnal eddy diffusivity
KE - kinetic energy density
MAXSLP - maximum allowable isopycnal slope
MMT - meridional overturning streamfunction
NHT - northward heat transport
TEMP - bottom temperature at 63N, 30W
VERTVIS - vertical eddy viscosity
WIND - peak value of the wind stress

REFERENCES

Bowman, K., J. Sacks and Y.-F. Chang. 1993. Design and analysis of numerical experiments. J. Atmos. Sci., *50,* 1267–1278.

Broecker, W. and T.-H. Peng. 1982. Tracers in the Sea. Lamont-Doherty Geological Observatory Publication (Palisades, New York).

Bryan, F. 1987. Parameter sensitivity of primitive equation ocean general circulation models. J. Phys. Oceanogr., *17,* 970–985.

Bryan, K. 1969. A numerical method for the study of the circulation of the world ocean. J. Comput. Phys., *4,* 347–376.

—— 1984. Accelerating convergence to equilibrium of ocean-climate models. J. Phys. Oceanogr., *14,* 666–673.

Bryan, K., S. Manabe and R. Pacanowski. 1975. A global ocean-atmosphere climate model. Part II. The oceanic circulation. J. Phys. Oceanogr., *5,* 30–45.

Cox, M. 1984. A primitive equation, three dimensional model of the ocean. GFDL Ocean Tech. Report No. 1, Princeton, NJ.

—— 1987. Isopycnal diffusion in a *z*-coordinate ocean model. Ocean Modelling, *74,* 1–5.

Cox, M. and K. Bryan. 1984. A numerical model of the ventilated thermocline. J. Phys. Oceanogr., *14,* 674–687.

Cummins, P., G. Holloway and A. Gargett. 1990. Sensitivity of the GFDL ocean general circulation model to a parameterization of vertical diffusivity. J. Phys. Oceanogr., *20,* 817–830.

England, M. E. 1992. On the formation of Antarctic Intermediate and Bottom Water in ocean general circulation models. J. Phys. Oceanogr., *22,* 918–926.

Gerdes, R., C. Koberle and J. Willebrand. 1991. The influence of numerical advection schemes on the results of ocean general circulation models. Clim. Dyn., *5,* 211–226.

Gough, W. A. 1991. Lateral and isopycnal mixing of passive and active tracers in an ocean general circulation model. Ph.D. thesis. McGill University, Montreal, Canada. 147 pp.

Gough, W. A. and C. A. Lin. 1992. The response of an ocean general circulation model to long time-scale surface temperature anomalies. Atmos.-Ocean, *30,* 653–674.

Haney, R. L. 1971. Surface thermal boundary conditions for ocean circulation models. J. Phys. Oceanogr., *1,* 241–248.

Holland, W. 1971. Ocean tracer distributions—a preliminary numerical experiment. Tellus, *23,* 371–392.

Iman, R. L. and W. J. Conover. 1982. A distribution-free approach to inducing rank correlation among input variables. Communi. Statistics Part B: Simulation and Computation, *11,* 311–334.

Killworth, P. D. 1989. On the parameterization of deep convection in ocean models, *in* Parameterization of Small-Scale Processes, P. Muller and D. Henderson, eds., Hawaii Institute of Geophysics Special Publication, University of Hawaii, 55–74.

Levitus, S. 1982. Climatological atlas of the world oceans. NOAA Prof. Paper 13, Washington, D.C.

Manabe, S., R. Stouffer, M. Spelman and K. Bryan. 1991. Transient response of a coupled ocean-atmosphere model to gradual changes of atmospheric CO_2. Part 1. Annual mean response. J. Climat., *4,* 785–818.

Marotzke, J. 1991. Influence of convective adjustment on the stability of the thermohaline circulation. J. Phys. Oceanogr., *21,* 903–907.

McDougall, T. 1987. Thermobaricity, cabbeling, and water-mass conversion. J. Geophys. Res., *92,* 5448–5464.

McDougall, T. and J. Church. 1986. Pitfalls with the numerical representation of isopycnal and diapycnal mixing. J. Phys. Oceanogr., *16,* 196–199.

McKay, M. D., W. J. Conover and R. J. Beckman. 1979. A comparison of three methods for selecting values of input variables in the analysis of output from a computer code, Technometrics, *21,* 239–245.

Montgomery, R. 1940. The present evidence on the importance of lateral mixing processes in the ocean. Bull. Amer. Met. Soc., *21,* 87–94.

Redi, M. 1982. Oceanic isopycnal mixing by coordinate rotation. J. Phys. Oceanogr., *12,* 1154–1158.

Sacks, J., S. B. Schiller, and W. J. Welch. 1989a. Designs for computer experiments. Technometrics, *31,* 41–47.

Sacks, J., W. J. Welch, T. J. Mitchell and H. P. Wynn. 1989b. Design and analysis of computer experiments (with discussion), Stat. Sci., *4,* 409–435.

Sarmiento, J. 1983. A simulation of bomb tritium entry into the Atlantic Ocean. J. Phys. Oceanogr., *13,* 1924–1939.

Stommel, H. 1958. The abyssal circulation. Deep-Sea Res., *5,* 80–82.

Veronis, G. 1975. The role of models in tracer studies, *in* Numerical models of Ocean Circulations, National Academy of Science, 133–146.

Weaver, A. J. and E. S. Sarachik. 1990. On the importance of vertical resolution in certain ocean general circulation models. J. Phys. Oceanogr., *20,* 600–609.

Welch, W. J., R. J. Buck, J. Sacks, H. P. Wynn, T. J. Mitchell and M. D. Morris. 1992. Screening, predicting, and computer experiments, Technometrics, *34,* 15–25.

Received: *9 September, 1993;* revised: *22 March, 1994.*